Molecular Cancer Therapeutics

Suppression of the Growth and Invasion of Human Head and Neck Squamous Cell Carcinomas via Regulating STAT3 Signaling and the miR-21/β-catenin Axis with HJC0152

Yu Wang[1], Sinan Wang[2], Yansheng Wu[1], Yu Ren[3], Zhaoqing Li[1], Xiaofeng Yao[1], Chao Zhang[4], Na Ye[5], Chao Jing[1], Jiabin Dong[1], Kailiang Zhang[6], Shanshan Sun[1], Minghui Zhao[1], Wenyu Guo[1], Xin Qu[1], Yu Qiao[1], Haiying Chen[5], Lingping Kong[1], Rui Jin[1], Xudong Wang[1], Lun Zhang[1], Jia Zhou[5], Qiang Shen[7], and Xuan Zhou[1]

Abstract

Signal transducer and activator of transcription 3 (STAT3) is involved in the tumor growth and metastasis of human head and neck squamous cell carcinoma (HNSCC) and is therefore a target with therapeutic potential. In this study, we show that HJC0152, a recently developed anticancer agent and a STAT3 signaling inhibitor, exhibits promising antitumor effects against HNSCC both *in vitro* and *in vivo* via inactivating STAT3 and downstream miR-21/β-catenin axis. HJC0152 treatment efficiently suppressed HNSCC cell proliferation, arrested the cell cycle at the G_0–G_1 phase, induced apoptosis, and reduced cell invasion in both SCC25 and CAL27 cell lines. Moreover, HJC0152 inhibited nuclear translocation of phosphorylated STAT3 at Tyr705 and decreased VHL/β-catenin signaling activity via regulation of miR-21. Loss of function of VHL remarkably compromised the antitumor effect of HJC0152 in both cell lines. In our SCC25-derived orthotopic mouse models, HJC0152 treatment significantly abrogated STAT3/β-catenin expression *in vivo*, leading to a global decrease of tumor growth and invasion. With its favorable aqueous solubility and oral bioavailability, HJC0152 holds the potential to be translated into the clinic as a promising therapeutic strategy for patients with HNSCC. *Mol Cancer Ther; 16(4); 578–90. ©2017 AACR.*

Introduction

Head and neck squamous cell carcinoma (HNSCC) is the sixth most common type of human cancer (1). Recently developed systemic therapies have improved outcomes, but the 5-year overall survival rate of patients with HNSCC remains at about 50% (2). More than 70% of patients with HNSCC suffer from relapsed or metastatic disease. There is an urgent need, therefore, for effective therapeutic regimens to treat HNSCC.

Signal transducer and activator of transcription 3 (STAT3) is implicated in cancer progression and tumor cell proliferation, invasion, and metastasis in human cancers of epithelial origin, including HNSCC (3). Triggered by upstream activation signals, STAT3 undergoes phosphorylation, homodimerization, nuclear translocation, and DNA binding, which then lead to transcription of various downstream target genes. Abundant evidence suggests that phosphorylation at the Tyr705 residue of STAT3 is abnormally activated in HNSCC and that pSTAT3 (Tyr705) could serve as a negative prognostic factor (4). STAT3 is, therefore, a promising therapeutic target. Inhibitors of STAT3 activation, including natural compounds, peptides, peptidomimetic compounds, chemically synthesized small molecules, and oligonucleotides, have been widely investigated (5–7). However, only a few of them have progressed into early-phase clinical trials. The majority of STAT3-inhibiting strategies fail because they exhibit only moderate tumor suppression, have poor aqueous solubility, or cause severe toxicity (8).

[1]Department of Maxillofacial and Otorhinolaryngological Oncology, Tianjin Medical University Cancer Institute and Hospital; Key Laboratory of Cancer Prevention and Therapy, Tianjin Cancer Institute; National Clinical Research Center of Cancer, Tianjin, China. [2]Department of Gastroenterology and Hepatology, Tianjin Medical University General Hospital; Tianjin Gastroenterology and Hepatology Institute, Tianjin, China. [3]Tianjin Research Center of Basic Medical Science, Tianjin Medical University, Tianjin, China. [4]Department of Genitourinary Oncology, Tianjin Medical University Cancer Institute and Hospital, Tianjin, China. [5]Chemical Biology Program, Department of Pharmacology and Toxicology, University of Texas Medical Branch, Galveston, Texas. [6]Department of Neurosurgery, Qilu Hospital of Shandong University, Brain Science Research Institute, Shandong University, Jinan, Shandong, China. [7]Department of Clinical Cancer Prevention, Division of Cancer Prevention and Population Sciences, The University of Texas MD Anderson Cancer Center, Houston, Texas.

Note: Supplementary data for this article are available at Molecular Cancer Therapeutics Online (http://mct.aacrjournals.org/).

Y. Wang, S. Wang, Y. Wu contributed equally to this article.

Corresponding Authors: Xuan Zhou, Department of Maxillofacial and Otorhinolaryngological Oncology, Tianjin Medical University Cancer Institute and Hospital; Key Laboratory of Cancer Prevention and Therapy, Tianjin Cancer Institute; National Clinical Research Center of Cancer, Tianjin 300060, China. E-mail: byron2000zhou@sina.com; Qiang Shen, Department of Clinical Cancer Prevention, The University of Texas MD Anderson Cancer Center, 6767 Bertner Avenue, BSRB S7.8136C, Houston, TX 77030. Phone: 713-834-6357; Fax: 717-834-6350; E-mail: qshen@mdanderson.org; and Jia Zhou, Chemical Biology Program, Department of Pharmacology and Toxicology, University of Texas Medical Branch, Galveston, TX 77555. E-mail: jizhou@utmb.edu

doi: 10.1158/1535-7163.MCT-16-0606

MicroRNA-21 (miR-21), a non-coding RNA, has been reported to regulate cell proliferation, apoptosis, and invasion in several human cancers (9–11). MiR-21 has been shown to be transcriptionally activated by the IL6/STAT3 signaling pathway in HNSCC (12), glioblastoma (13), leukemia (14), and multiple myeloma (15). In addition, miR-21 is involved in β-catenin signaling regulation through direct targeting of the von Hippel–Lindau gene (VHL; ref. 16). The VHL/β-catenin axis contributes to cancer invasion and metastasis in HNSCC (17), glioblastoma (16, 18), and renal cell carcinoma (19). Our previous findings have also revealed that the VHL/β-catenin axis regulates the epithelial–mesenchymal transition (EMT) in HNSCC and may, therefore, be a therapeutic target (17).

Niclosamide, an FDA-approved anticestodal drug, has recently proven effective in the suppression of STAT3 signaling (20). However, its pharmacokinetic profile is limited because of its poor aqueous solubility and oral bioavailability. HJC0152, an *O*-alkylamino-tethered derivative of niclosamide, was designed to be a more potent STAT3 signaling inhibitor and has shown better water solubility and oral bioavailability *in vivo* (21). Based on these, we hold *in vitro* and *in vivo* experiments to determine whether it is possible for HJC0152 to be a candidate for HNSCC therapy. In the present study, we show that HJC0152 exerted a significant anticancer effect on HNSCC tumor growth and invasion. We further identified STAT3 activation and the miR-21/β-catenin axis as the predominant targets at which HJC0152 exerts its anti-HNSCC effects.

Materials and Methods

Chemicals and reagents

We previously designed and synthesized HJC0152, and its structure was published (21). For *in vitro* experiments, a stock solution was prepared in 100% dimethyl sulfoxide (DMSO; Sigma) at a concentration of 10 mmol/L. For *in vivo* experiments, drugs were dissolved in 7.5 mg/kg DMSO as previously described (21).

Cell lines and culture conditions

Human SCC25, CAL27, and UM1 HNSCC cell lines were obtained from ATCC. Hep-2 and TSCCA cells were purchased from the Institute of Basic Medical Sciences, Chinese Academy of Medical Sciences. The Tb3.1 tongue squamous cell carcinoma cell line was a gift of Professor Chenping Zhang at Shanghai Jiaotong University. All the cell lines were maintained in Dulbecco's modified Eagle's medium (DMEM, Gibco), DMEM/Ham's F-12 (Gibco), or RPMI-1640 (Gibco), respectively, each supplemented with 10% FBS (Gibco) and penicillin (100 U/mL)/streptomycin (100 μg/mL) (HyClone). All cells were maintained under humanized conditions (37°C, 5% CO_2) and were regularly checked for *Mycoplasma* contamination. Cell lines were authenticated by array comparative genomic hybridization or DNA fingerprinting.

Cell growth and viability assay

SCC25 or CAL27 cells (5,000 cells/well) were seeded into 96-well plates and incubated at 37°C for 24 hours to allow for stabilization, and then exposed to HJC0152 (0.1, 0.5, 1, 2, 4, 6, 8, 10 μmol/L) or DMSO (1 μL/well) for 24 hours. Cell viability was measured by an MTT assay (5 mg/mL; Sigma). The MTT crystals were dissolved in DMSO, and the absorbance at 490 nm was assessed using a microplate reader (Model 680, Bio-Rad Laboratories Ltd.). IC_{50} was calculated using SPSS software (version 17.0).

Transwell and wound-healing assays

For *in vitro* invasion and migration assays, SCC25 or CAL27 cells (50,000 cells/well) were plated into Transwell inserts (Corning) that had been coated with Matrigel (BD Biosciences) or left uncoated. The lower chambers were filled with medium plus 20% FBS. After incubation at 37°C for 16 hours, the penetrated cells were fixed with 4% paraformaldehyde (Solarbio) and stained with 0.1% crystal violet (Solarbio). Each image was observed using an inverted microscope (DMI6000B, Leica).

A wound-healing assay was used to confirm the result of the Transwell assay. We added 500,000 SCC25 or CAL27 cells into 6-well plates. When the cells had grown to approximately 80% confluence, we made scratches using 10-μL pipette tips, creating a wound field of approximately 400 mm wide, based on the scaleplate in the microscope. The plates were incubated in fresh medium (without FBS) for 48 hours. Images of gaps from several randomly selected fields were acquired at the start (0 hours), halfway point (24 hours), and endpoint (48 hours) of the experiment, using an inverted microscope (DMI6000B, Leica).

Clonogenicity assay

SCC25 or CAL27 cells (500 cells/well) were seeded in 2 mL of growth medium with 10% FBS in a 6-well plate overnight. The cells were incubated for 14 days in the presence or absence of HJC0152 (2 μmol/L for SCC25 and 1 μmol/L for CAL27) at 37°C in 5% CO_2 and then washed twice in PBS and stained with 0.1% crystal violet. Colonies with > 50 cells per a specific size of field were counted under an inverted microscope (DMI6000B, Leica).

Reverse-transcription PCR

Total RNAs were extracted using TRIzol (Invitrogen) according to the manufacturer's instructions and were reverse transcribed to cDNA by using the PrimeScript 1st Strand cDNA Synthesis Kit (KeyGEN BioTECH). Ten nanograms of reverse-transcribed products was then detected with quantitative real-time PCR (qRT-PCR; Bio-Rad) as described previously (22). U6 was used as a loading control, and the $2^{-\Delta\Delta Ct}$ method was used to evaluate the relative abundance of genes. Primers for U6 and miR-21 are shown in Supplementary Table S1.

Flow cytometry

To analyze apoptosis rates, CAL27 and SCC25 cells were treated with DMSO or HJC0152 (1 μmol/L for CAL27 and 2 μmol/L for SCC25) and then digested with trypsin (Gibco) and resuspended as single-cell suspensions. Double staining with fluorescein isothiocyanate (FITC)–Annexin V and propidium iodide (PI) was conducted in accordance with the manufacturer's instructions (BD Biosciences). Apoptosis was measured using flow cytometry (FACSCanto II, BD Biosciences).

To determine cell-cycle distribution, cells treated with DMSO or HJC0152 (2 μmol/L for SCC25 and 1 μmol/L for CAL27) were trypsinized, fixed in 75% ethanol, washed twice with PBS, and incubated with 50 μL PI (1 μg/μL) and 0.5 μL RNase (100 μg/μL; KeyGEN BioTECH) for 30 minutes in the dark. Cells were then evaluated using flow cytometry (FACSCanto II, BD Biosciences).

Western blotting

After treatment, cell lysates were prepared in radioimmunoprecipitation assay buffer (Solarbio) supplemented with protease and phosphatase inhibitors (Roche). The lysates were then centrifuged (15,000 × *g*, 4°C) for 30 minutes to remove cellular debris. Protein concentrations were determined by a BCA protein assay kit (Micro BCA Protein Assay Kit, ThermoFisher Scientific). We boiled 20 to 30 μg of each protein sample for 5 minutes and resolved the proteins in 8%, 10%, or 15% gradient SDS-PAGE gels (Solarbio). After gel electrophoresis, the proteins were transferred to polyvinylidene difluoride membranes (Merck Millipore). The membranes were blocked in 5% non-fat milk in TBS containing 0.1% Tween 20 (TBST) at room temperature for 2 hours and then incubated with primary antibodies overnight at 4°C in TBST containing 5% non-fat milk. The membranes were then washed twice with TBST and incubated with horseradish peroxidase-conjugated secondary antibodies in a 5% non-fat milk/TBST solution for 1 hour at room temperature. ImageJ software (NIH) was used to quantify the relative expression levels of the target proteins, normalized to the respective internal controls. The primary antibodies used in this experiment are listed in Supplementary Table S2.

IHC and immunofluorescence staining

For IHC staining, paraffin-embedded HNSCC tissue samples (*in vivo*) were deparaffinized, rehydrated, and incubated with primary antibodies (1:100 dilutions) overnight at 4°C. The slides were then incubated with a biotin-labeled secondary antibody (1:100 dilutions) for 40 minutes at 37°C. Cells were visualized using a Vectastain ABC kit and a DAB Chromogen kit (Vector Laboratories). The primary antibodies used in this investigation are listed in Supplementary Table S1.

For immunofluorescence staining, HNSCC cells were grown on 18-mm cover glasses and treated with HJC0152 for 24 hours. Immunofluorescence staining was conducted with primary antibodies against STAT3, pSTAT3 (Tyr705; 1:100 dilutions, Abcam), and β-catenin (1:100 dilutions, Cell Signaling Technology). The cells were then washed with PBS and incubated with Alexa Fluor 488 or Alexa Fluor 594 secondary antibodies (Cell Signaling Technology). The nuclei were stained with 4,6-diamidino-2-phenylindole (DAPI; ThermoFisher Scientific), and each slide was visualized using an FV-1000 laser scanning confocal microscope (Olympus).

Gelatin zymography

HNSCC cell lines were seeded at a density of 5×10^5 cells per well in 6-well plate. Cells were incubated in serum-free DMEM for 24 hours, with or without HJC0152 (2 μmol/L for SCC25 and 1 μmol/L for CAL27 cells). Culture supernatants were collected and then diluted with zymography buffer (P1700, APPLYGEN). A total of 20 μg of protein per lane was loaded onto 10% SDS gels containing 1 mg/mL gelatin (P1700, APPLYGEN). After electrophoresis, each gel was washed twice for 30 minutes each with 2.5% Triton X-100 at room temperature and then was incubated in zymography buffer (P1700, APPLYGEN) overnight at 37°C. Each gel was then stained in 50 mL Coomassie brilliant blue R-250 (P1700, APPLYGEN), followed by treatment of destaining buffer (30% methanol, 10% glacial acetic acid, 60% distilled water). A clear white band showing MMP-2/9 activity was detected against a blue background. The gels were photographed with ChemiDoc XRS Imaging System (Bio-Rad).

RNA transfection

SCC25 or CAL27 cells transfected with negative control (NC) oligos or miR-21 mimics (20 nmol/L; Genepharma) were labeled as NC or miR-21, respectively. HNSCC cells transfected with si-NC or siRNAs (20 nmol/L; RIBOBIO) against STAT3 or VHL, labeled as si-NC, si-STAT3, or si-VHL, respectively, using Lipofectamine 2000 reagent according to the manufacturer's instructions (Life Technology). During transfection, Opti-MEM medium without FBS was used, and the transfected medium was replaced with DMEM-F12 or DMEM after 6 hours. The sequences of both the miRNAs and siRNAs are listed in Supplementary Table S1.

Luciferase reporter assay

To evaluate β-catenin/transcription factor 4 (TCF-4) transcriptional activity, we used the TOP-FLASH and FOP-FLASH luciferase reporter constructs (Merck Millipore). TOP-FLASH (with three repeats of the TCF binding site, 40 ng/well) or FOP-FLASH (with three repeats of a mutated TCF binding site, 40 ng/well) plasmids were transfected into cells treated with DMSO or HJC0152, respectively. For the reporter assay, SCC25 and CAL27 cells (5,000 cells/well) were cultured in 96-well plates. After 24 hours, luciferase activity was assessed with a Dual-Luciferase Reporter Assay (Promega). The Renilla luciferase activity was used as an internal control (22).

In vivo orthotopic tumor model

A total of 5×10^6 SCC25 cells that had been infected with a luciferase lentivirus (Promega) and stably expressed luciferase were injected into the base of the tongues of 4-week-old BALB/c-nu mice (23, 24). Because the SCC25 cell line was derived from a 70-year-old male patient and HNSCC had a male predominance (25), we used 10 male mice for further analysis. The animals were obtained from the Institute of Zoology of Concorde Blood Institute (Tianjin, China). To verify tumor establishment, fluorescence images were captured 7 days after the injection with an IVIS Lumina Imaging System (Caliper Life Sciences; ref. 24). The mice were randomly assigned to either a DMSO (control) or HJC0152 (7.5 mg/kg) treatment group (5 mice per group; ref. 21). All these mice were treated daily with 7.5 mg/kg HJC0152 (HJC0152 group) and DMSO (DMSO group) intraperitoneally. Bioluminescence imaging for tumor volume were collected each week, and body weight was measured daily. After 28 days, the animals were sacrificed by cervical dislocation under anesthesia and the orthotopic tumors were collected for further pathological examination. Tumor specimens were used for IHC and terminal deoxynucleotidyl transferase dUTP nick end labeling (TUNEL) assays. All animal study protocols were approved by the Institutional Animal Care and Use Committee of Tianjin Medical University Cancer Institute and Hospital.

TUNEL assay

Apoptosis in the tumor specimens was detected by a TUNEL assay using an *in situ* cell death kit (Roche), following the manufacturer's protocol. The nuclei were counterstained with DAPI reagent for 1 hour, and the slides were stored at −80°C. Positively stained cells were visualized using an FV-1000 laser scanning confocal microscope.

Statistical analysis

SPSS software (version 17.0) was used for the statistical analyses. Statistical comparisons between two groups were made

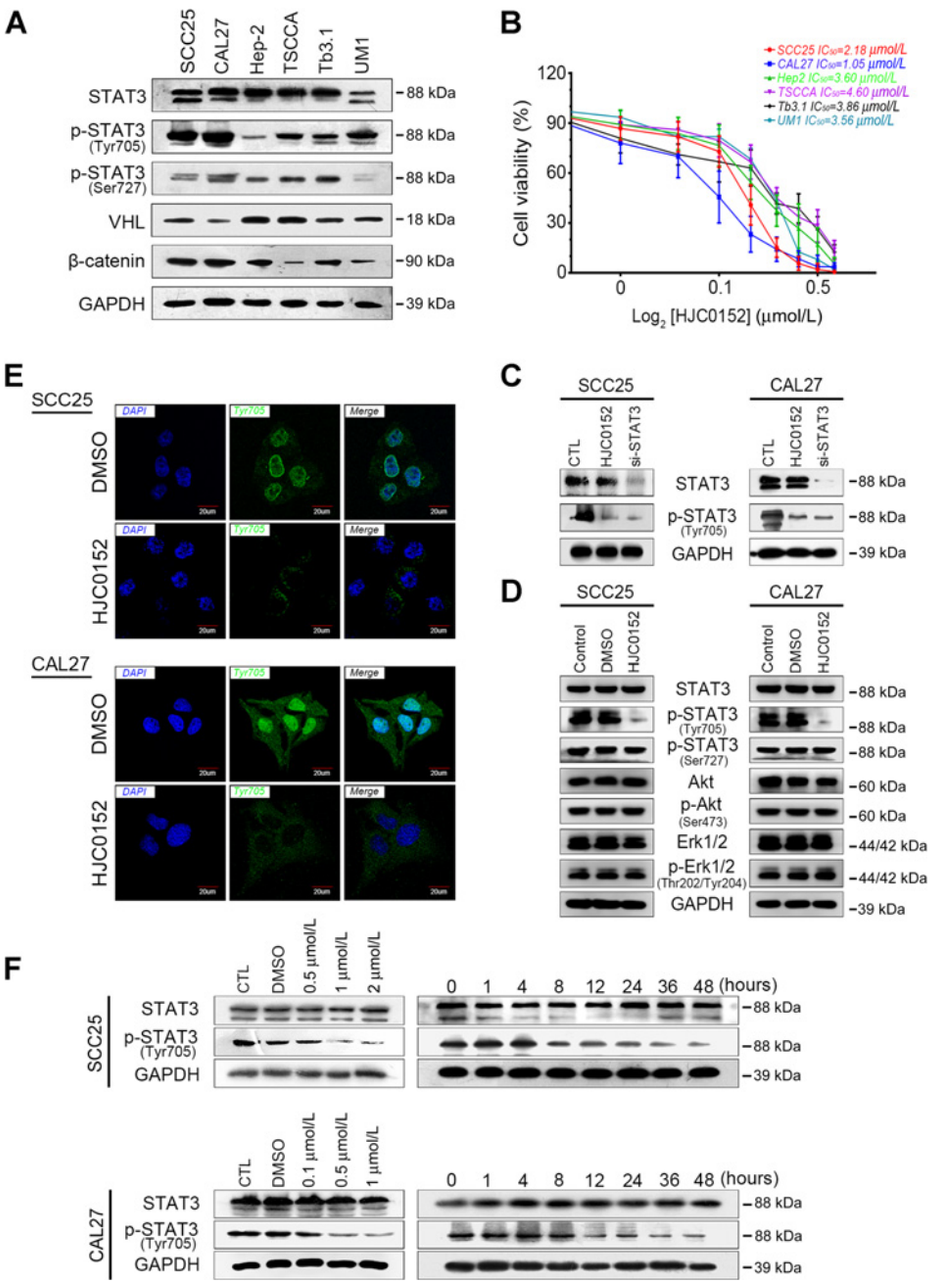

Figure 1.

HJC0152 specifically inhibits STAT3 activity in HNSCC cells. **A,** STAT3, p-STAT3 (Tyr705), p-STAT3 (Ser727), VHL, and β-catenin expression was determined by Western blot analysis in six HNSCC cell lines. **B,** Cell survival percentage was measured by an MTT assay after treatment of HNSCC cell lines with HJC0152 for 24 hours (error bars, standard deviation). **C,** Western blotting showed that HJC0152 (2 μmol/L for SCC25 and 1 μmol/L for CAL27 cell lines) selectively inhibited p-STAT3 (Tyr705), but not STAT3, in HNSCC cell lines. **D,** HNSCC cell lines were treated with HJC0152 at various concentrations (2 μmol/L for SCC25 and 1 μmol/L for CAL27 cell lines) for 24 hours. Cells were lysed for Western blot analysis using antibodies specific to p-Stat3, Stat3, p-Akt, Akt, p-Erk1/2, Erk1/2, and GAPDH. **E,** p-STAT3 (Tyr705) was detected via immunofluorescence staining 24 hours after SCC25 and CAL27 cells were treated with HJC0152 (2 μmol/L for SCC25 and 1 μmol/L for CAL27 cell lines) or DMSO. An anti-rabbit antibody against p-STAT3 was used for labeling (scale bar, 20 μm). **F,** HJC0152 significantly inhibited p-STAT3 (Tyr705) expression in a dose- and time-dependent manner, as assessed by immunoblotting. GAPDH was used as a loading control.

using a Student *t* test. Differences among groups were determined by two-way ANOVA followed by a Dunnett test. All data were expressed as means ± SD and represented the average of at least three experiments performed in triplicate. A P value < 0.05 was considered statistically significant.

Results

HJC0152 specifically inhibits phosphorylation and nuclear accumulation of STAT3 in HNSCC cells *in vitro*

The SCC25 and CAL27 cell lines showed higher levels of p-STAT3 (Tyr705) than did the Hep-2, TSCCA, Tb3.1, and UM1 cell lines (Fig. 1A). As shown in Fig. 1B, the CAL27 (IC_{50} = 1.05 μmol/L) and SCC25 (IC_{50} = 2.18 μmol/L) cell lines displayed higher sensitivity to HJC0152 than did the other cell lines, suggesting that HNSCC cell lines with higher p-STAT3 (Tyr705) expression levels are more sensitive to HJC0152. These results led us to select SCC25 and CAL27 cells for further investigation.

We used two STAT3 siRNAs (si#1 and si#2) to block STAT3 and p-STAT3 (Tyr705); both dramatically inhibited the expression of STAT3 and p-STAT3 (Tyr705). Because it had better knockdown efficiency, we selected si#2 for further analysis (Supplementary Fig. S1A). In HJC0152-treated CAL27 and SCC25 cells, p-STAT3 (Tyr705) expression was significantly lower than that in untreated control cells, but no difference in total STAT3 expression was found (Fig. 1C). Moreover, HJC0152 and si-STAT3 both dramatically inhibited tumor cell proliferation, migration and invasion

in vitro (Supplementary Fig. S1B–S1D, $P < 0.05$). To determine the selectivity and specificity of HJC0152 on STAT3 signaling inhibition, AKT and MAPK (Erk1/2), two important signaling proteins, were assessed. Western blots were used to detect the expression level of total and phosphorylated STAT3, AKT, and MAPK (Erk1/2; Fig. 1D). In contrast to attenuation of phosphorylation of STAT3 (Fig. 1C and D), phosphorylation of AKT and MAPK (Erk1/2) was not inhibited in both HNSCC cell lines tested (Fig. 1D). These observations suggest that HJC0152 specifically inhibits STAT3 signaling, but not AKT and MAPK signaling, in HNSCC cells. Immunofluorescence staining showed that p-STAT3 (Tyr705) levels were lower in HJC0152-treated CAL27 and SCC25 cells, with higher p-STAT3 (Tyr705) accumulation in the cytoplasm than in the nucleus (Fig. 1E and Supplementary Fig. S2B). Moreover, immunofluorescence analysis revealed no significant change in total STAT3 staining in either cell line (Supplementary Fig. S2A and S2B). Additionally, as shown in Fig. 1D, HJC0152 treatment did not affect p-STAT3 (Ser727) levels in CAL27 and SCC25 cell lines. We also found that HJC0152 inhibited p-STAT3 (Tyr705) in HNSCC cells in a dose- and time-dependent manner (Fig. 1F).

HJC0152 reduces invasion and migration in HNSCC cell lines

We next measured the effect of HJC0152 treatment on cell migration and invasion in HNSCC cell lines. Results from the Transwell assays suggested that HJC0152 significantly inhibits SCC25 and CAL27 cell migration ($P < 0.05$, respectively, without Matrigel) and invasion (with Matrigel) in a dose-dependent manner. Higher doses of HJC0152 had stronger effects on tumor cell migration and invasion capacity (Fig. 2A). The scratch test demonstrated that HJC0152 delayed wound healing in both HNSCC cell lines (Supplementary Fig. S3A, $P < 0.05$), suggesting that HJC0152 inhibits the invasion and migration capacities of HNSCC cells.

In order to further study the underlying mechanisms of HJC0152's inhibition of cell invasion and migration, we next measured expression of matrix metalloproteinases before and after HJC0152 treatment. MMP2/9 enzymes were regarded as biomarkers of cancer invasion and metastasis (26, 27). Moreover, STAT3 transcriptionally regulates the expression of MMP2 (26, 28–30) and MMP9 (14, 27, 31, 32). In both cell lines tested, HJC0152 treatment significantly inhibited the expression and secretion of MMP2/9, suggesting that HJC0152 attenuates MMP2/9's ability to degrade the extracellular matrix (Fig. 2B and Supplementary Fig. S3B). Additionally, EMT was widely regarded as one of the most important mechanisms of cancer metastasis (33–39), and we thus hypothesized that HJC0152 might inhibit HNSCC invasion and metastasis via EMT interruption. As shown in Fig. 2B, we found that the important EMT markers N-cadherin, vimentin, and Twist-1 were effectively inhibited in HJC0152-treated cells. Furthermore, the subsequent immunofluorescence staining indicates the gain of E-cadherin and loss of N-cadherin following HJC0152 administration, similar to the findings in Western blot assays (Fig. 2C). Taken together, these data reveal that HJC0152 treatment inhibits tumor cell migration and invasion *in vitro* by interrupting the EMT process.

HJC0152 suppresses cell proliferation and induces apoptosis in HNSCC cells *in vitro*

Uncontrolled cell proliferation and apoptosis resistance are considered to be the most important characteristics of tumor cells. We investigated the effect of HJC0152 on tumor cell growth *in vitro*. As shown by the clonogenicity assay, after 14 days of continuous HJC0152 treatment, both the size and the number of SCC25 and CAL27 clones were reduced. The clone density of SCC25 ($P < 0.05$) and CAL27 ($P < 0.05$) cells (per 100 mm^2) was reduced by HJC0152 treatment. These results suggest that HJC0152 has an antiproliferative effect on HNSCC cells (Fig. 3A). In the MTT assay, HJC0152-treated SCC25 (2 μmol/L) and CAL27 (1 μmol/L) cells showed approximately 50% of the number of viable cells found in the DMSO group at 24 hours after treatment. Cell viability reached its lowest level at 72 hours and then leveled off (Fig. 3E, $P < 0.05$). Taken together, these results suggest that HJC0152 inhibits the proliferation of HNSCC cells in both dose- and time-dependent manners.

Cell-cycle analysis was performed to further understand the mechanism of HJC0152 in the inhibition of cell proliferation. As shown in Fig. 3B, we observed an increase in the accumulation of cells in the G_1 phase in SCC25 ($P < 0.05$) and CAL27 ($P < 0.05$) cell lines treated with increasing concentrations of HJC0152 for 24 hours. Expression of the cell cycle–related molecule Cyclin-D1 was remarkably suppressed, while expression of the cyclin-dependent kinase inhibitor p21 was upregulated (Fig. 3D). These results were consistent with those of the flow cytometric analysis.

We next used FITC–Annexin V/PI staining to assess apoptosis rates in the HNSCC cell lines after HJC0152 exposure. As shown in Fig. 3C, HJC0152 significantly induced apoptosis in both SCC25 ($P < 0.05$) and CAL27 ($P < 0.05$) cell lines. We also evaluated the expression levels of several apoptosis-related proteins by Western blot 24 hours after HJC0152 treatment (Fig. 3D). As expected, the B-cell lymphoma 2-family protein BCL-2, a regulator of apoptosis, was decreased, while the BCL-2–associated X protein (BAX) was increased. Expression levels of cleaved caspase-3 also rose with increasing drug concentrations. These results suggest that HJC0152 significantly induces G_0–G_1 phase arrest and caspase-dependent apoptosis in HNSCC cells.

HJC0152 regulates the activity of the STAT3/miR-21/β-catenin axis

It has been widely reported that miR-21 is upregulated by IL6/STAT3 activation in glioma (13), chronic lymphocytic leukemia (14), HNSCC (12), and multiple myeloma (15). Because HJC0152 affected HNSCC cells via p-STAT (Tyr705) inhibition (Fig. 1C and D), we investigated the role of STAT3/miR-21 signaling in the mechanism of HJC0152. In our results, miR-21 expression levels were remarkably decreased after HJC0152 treatment in both cell lines (Fig. 4A, $P < 0.05$). qRT-PCR showed that in both cells that were transfected with si-STAT3 and those that were exposed to HJC0152, miR-21 was attenuated (Supplementary Fig. S4A, $P < 0.05$). Subsequently, SCC25 and CAL27 cells were transfected with miR-21 mimics for 3 days. qRT-PCR revealed that miR-21 expression was significantly elevated (Supplementary Fig. S4B, $P < 0.05$), VHL expression was decreased, and β-catenin levels were increased (Supplementary Fig. S4C). These results reveal that miR-21 plays an essential regulating role in VHL/β-catenin signaling in HNSCC cell lines.

To clarify the role of the STAT3/miR-21/β-catenin axis in the mechanism of HJC0152, we used Western blotting. As shown in Supplementary Fig. S4D, HJC0152 mimicked the effect of siRNA on the VHL/β-catenin axis. We also found that VHL expression was upregulated and β-catenin attenuated by HJC0152 in dose- and time-dependent manners (Fig. 4B).

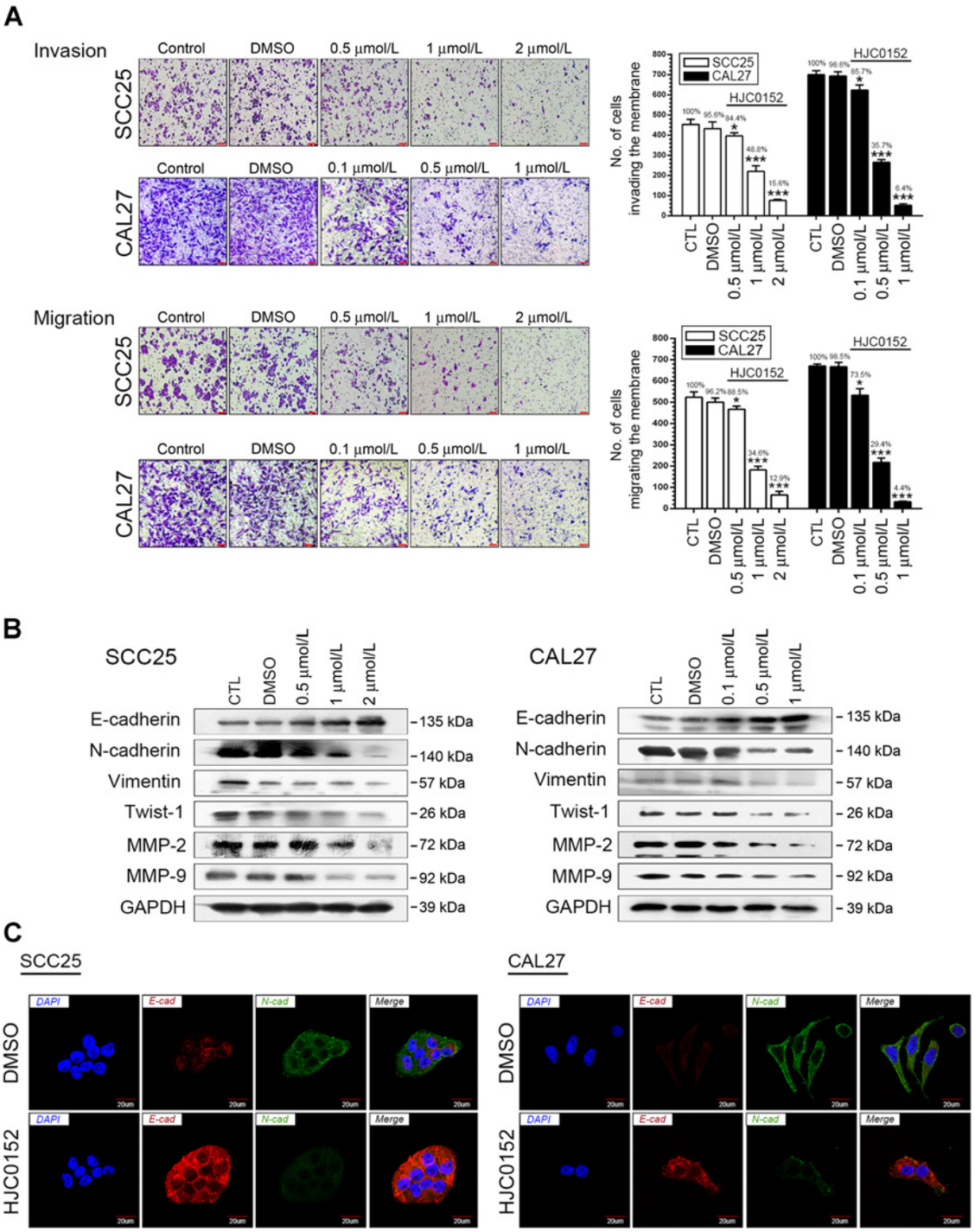

Figure 2.

HJC0152 reduces the invasiveness of HNSCC cells *in vitro*. **A,** A Transwell assay showed that HJC0152 dramatically attenuated the migration (without Matrigel) and invasion capacity (with Matrigel) of SCC25 and CAL27 cells. Cells were seeded in the top compartment of a Transwell chamber and left untreated (control) or treated with DMSO or HJC0152 for 24 hours ($P < 0.05$, scale bar, 100 μm). **B** and **C,** SCC25 and CAL27 cells were treated with HJC0152 for 24 hours, and the expression of EMT-related proteins was analyzed by both Western blot and immunofluorescence. *, $P < 0.05$; ***, $P < 0.001$.

When we treated SCC25 and CAL27 cells with HJC0152 and transfected them with si-VHL for 3 days, we found that VHL abrogation significantly attenuated the effects of HJC0152 on β-catenin and reversed HJC0152's anticancer effects on cell proliferation and migration *in vitro* (Fig. 4C and D and Supplementary Fig. S5A and S5B, $P < 0.05$).

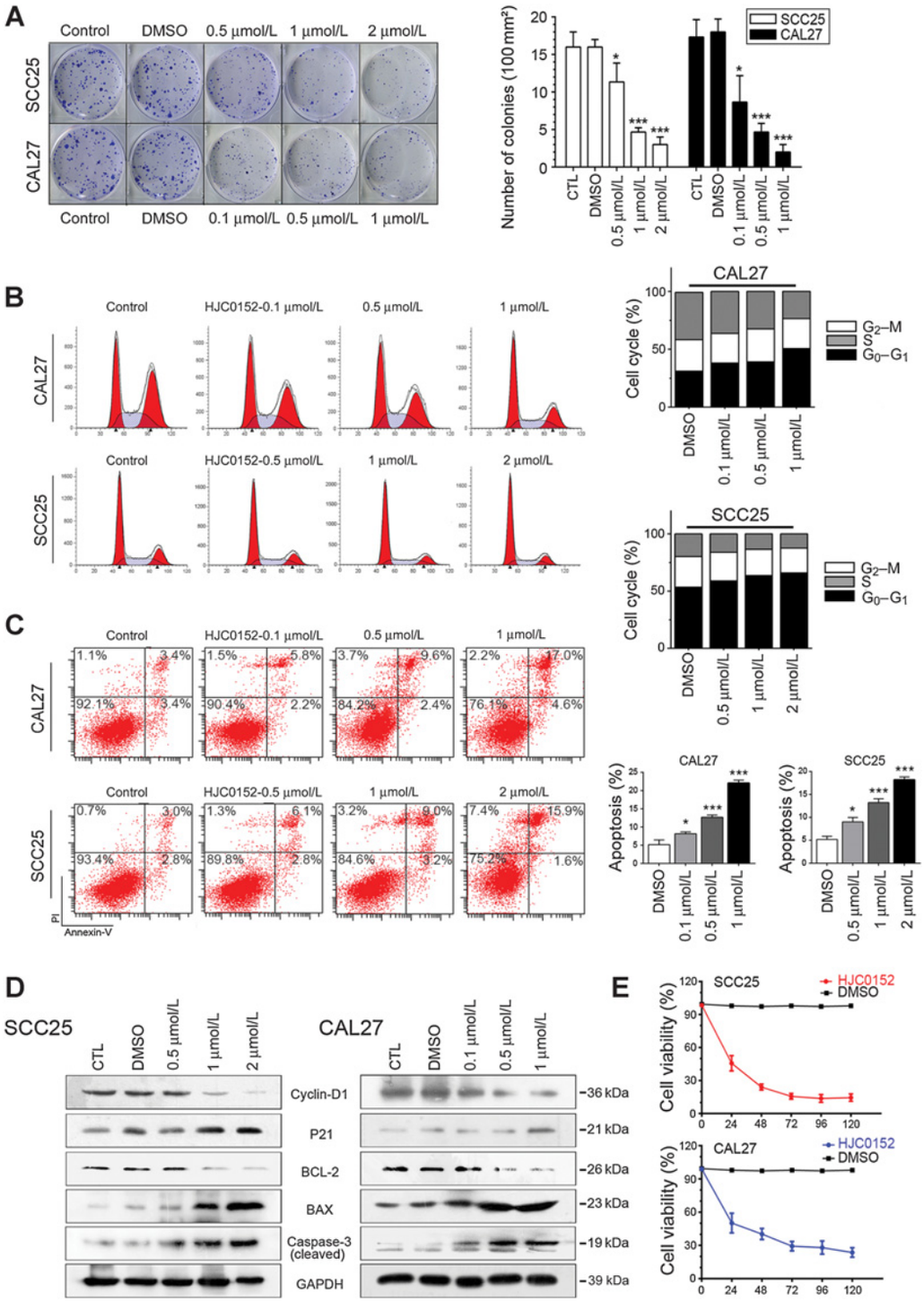

Figure 3.

HJC0152 suppresses proliferation and induces apoptosis in HNSCC cells. **A,** Reduction of clone formation ability in HJC0152-treated SCC25 and CAL27 cells. **B,** HJC0152-induced G_0–G_1 phase arrest of SCC25 and CAL27 cells ($P < 0.05$). **C,** Annexin V/propidium iodide (PI) staining showing that the percentage of apoptotic cells was significantly increased by HJC0152 treatment in a dose-dependent manner. **D,** SCC25 and CAL27 cells were treated with HJC0152 for 24 hours, and the expression levels of cell cycle– and apoptosis-related proteins were analyzed by Western blotting. **E,** Cell viability of SCC25 and CAL27 cell lines were significantly impaired after HJC0152 treatment for 72 hours (scale bar, 100 μm). Cells were treated with HJC0152 or DMSO for 1, 2, 3, 4, 5 days, respectively, and then measured by MTT assay ($P < 0.05$). *, $P < 0.05$; ***, $P < 0.001$.

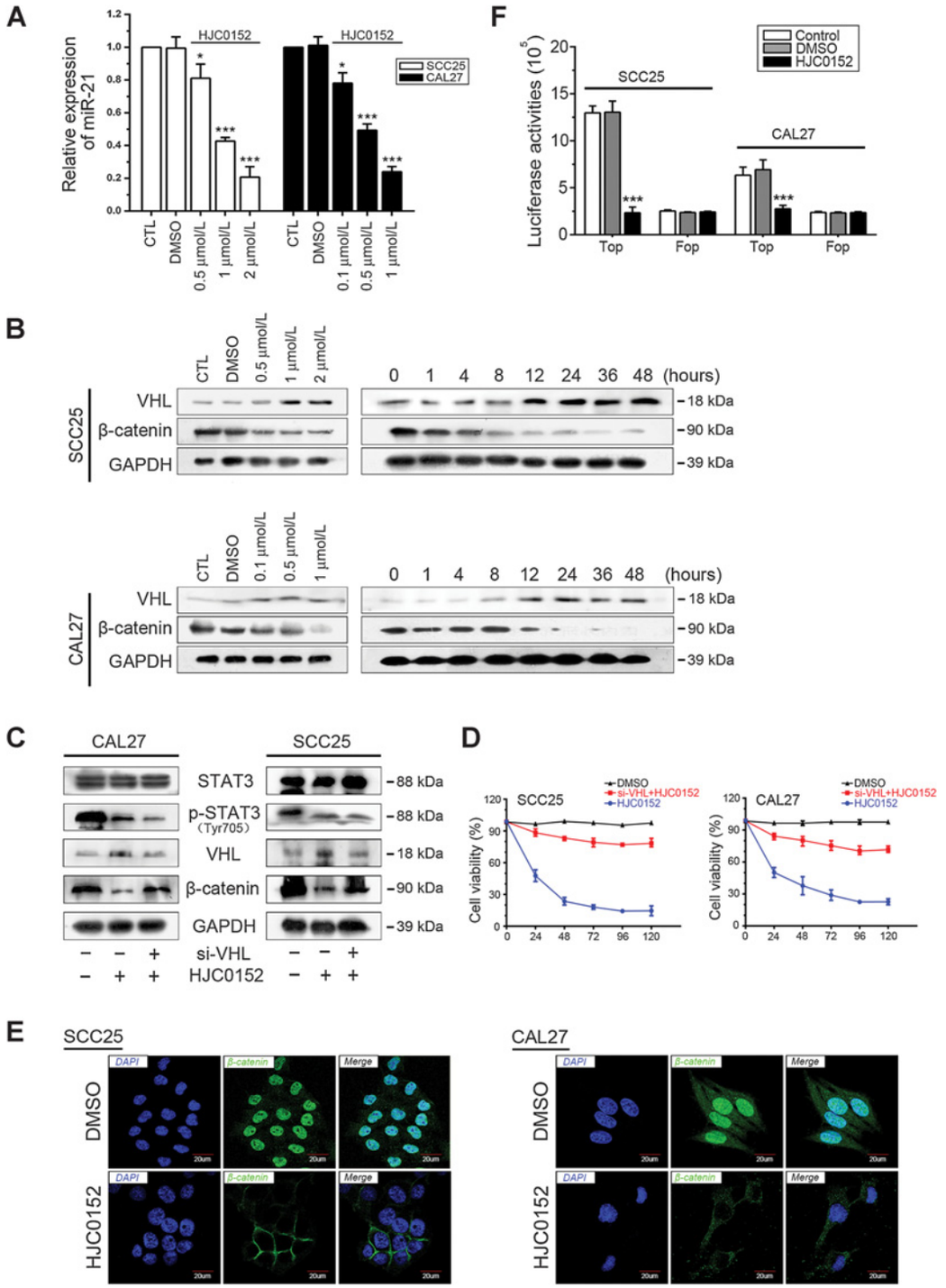

Figure 4.

HJC0152 regulates the activity of miR-21/β-catenin signaling. **A,** miR-21 expression was quantified by qRT-PCR analysis (normalized to U6 RNA). HJC0152 attenuated the expression of miR-21 in a dose-dependent manner in HNSCC cell lines ($P < 0.05$). **B,** HJC0152 inhibited β-catenin activity in HNSCC cell lines in a dose- and time-dependent manner and elevated VHL expression levels. **C,** Transfection with si-VHL significantly reduced VHL expression in HNSCC cells and counteracted the impact of HJC0152 (2 μmol/L for SCC25 and 1 μmol/L for CAL27 cell lines) on VHL/β-catenin signaling. **D,** si-VHL dramatically compensated the antitumor effect of HJC0152 on cell viability, measured by MTT assay. **E,** Immunofluorescence detection, 24 hours after treatment of SCC25 (2 μmol/L) and CAL27 (1 μmol/L) cells with HJC0152 or DMSO, showed that HJC0152 dramatically blocked the nuclear translocation of β-catenin. An anti-rabbit antibody against β-catenin was used for labeling (scale bar, 20 μm). **F,** SCC25 and CAL27 cells were transfected with a TOP/FOP plasmid. After cells were treated with HJC0152 (2 μmol/L for SCC25 and 1 μmol/L for CAL27 cell lines) for 24 hours, luciferase reporter assays were performed. *, $P < 0.05$; ***, $P < 0.001$.

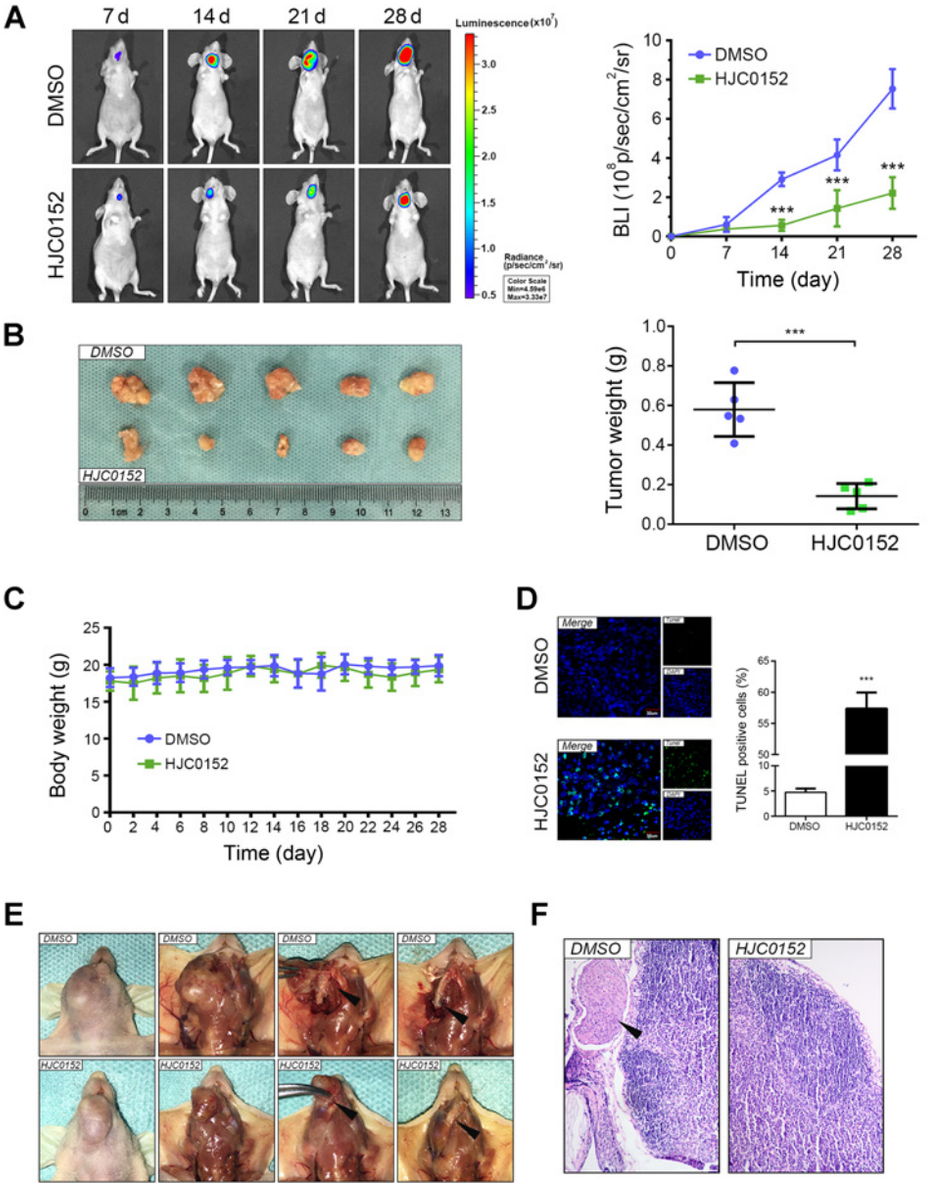

Figure 5.
HJC0152 slows HNSCC tumor growth and suppressed local invasion *in vivo*. **A,** Representative bioluminescence images comparing HJC0152-treated (7.5 mg/kg) orthotopic HNSCC tumors with DMSO-treated controls every week for 4 weeks (BLI: bioluminescence imaging, $P < 0.05$). **B,** Representative images for orthotopic tumors of HJC0152 or DMSO-treated animals. **C,** Based on body weight, no detectable toxicity was observed at the tested dose (7.5 mg/kg; error bars, SD). **D,** A TUNEL assay showed more induced apoptotic nuclei in HJC0152-treated tumor cells (7.5 mg/kg) than in DMSO-treated cells (scale bar, 30 μm). **E,** Representative photographs of the tumor resection procedure. HJC0152 (7.5 mg/kg) significantly inhibited local invasion of orthotopic HNSCC tumors. In each group, the first two photographs represent the original orthotopic tumor while the last two photographs represent the local invasion situation during and after resection, respectively. **F,** HJC0152 (7.5 mg/kg) significantly inhibited cervical lymph node metastasis of orthotopic HNSCC tumors.
*, $P < 0.05$; ***, $P < 0.001$.

HJC0152 also dramatically blocked the nuclear translocation of β-catenin, as assessed by immunofluorescence assays and Western blot of cytosolic/nuclear fractionation (Fig. 4E and Supplementary Fig. S2B). A TOP/FOP-FLASH luciferase assay was used to detect the transcriptional activity of β-catenin. In HNSCC cell lines, HJC0152 significantly reduced TOP-FLASH luciferase activity ($P < 0.05$) but did not change FOP activity (Fig. 4F). Taken together, these results suggest that HJC0152 exerts its antitumor effect via the STAT3/miR-21/β-catenin axis in HNSCC.

HJC0152 reduces HNSCC tumor growth and invasion *in vivo*

In order to further validate the antitumor effect and clinical potential of HJC0152, we developed an orthotopic HNSCC tumor model derived from the SCC25 cell line. HJC0152-treated (7.5 mg/kg) tumors showed significantly lower tumor volume (Fig. 5A and B, $P < 0.05$) and tumor weight (Fig. 5B, $P < 0.05$) than did DMSO-treated tumors. More importantly, no significant change in body weight (Fig. 5C) was observed in the mice treated with HJC0152 compared with the DMSO group. We employed a TUNEL assay to examine DNA fragmentation, the hallmark of apoptotic cells (Fig. 5D), in tumor samples. The results demonstrated that more HJC0152-treated cells had apoptotic nuclei than did DMSO-treated cells ($P < 0.05$). Furthermore, we found that Ki-67, cyclin D1, and BCL-2 expression were all dramatically attenuated and that cleaved caspase-3 was significantly upregulated in HJC0152-treated tumors *in vivo* (Fig. 6B).

Figure 5E and F show that HJC0152-treated mice had lower levels of local invasion and lymph node metastasis than did DMSO-treated mice, assessed by local resection, observation and subsequent HE staining. Besides, according to IHC, MMP2/9

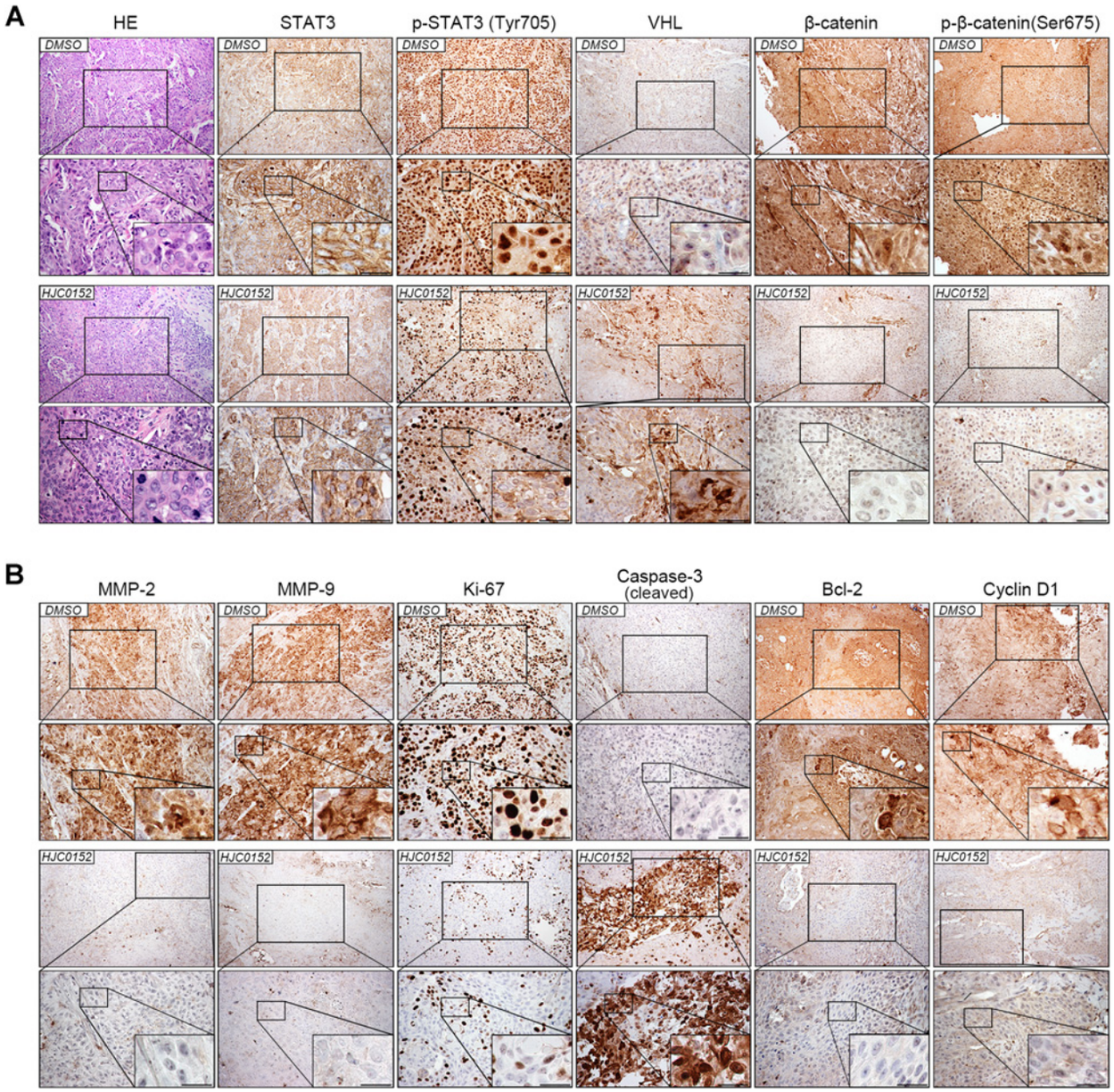

Figure 6.

HJC0152 exerts antitumor effect *in vivo* via targeting STAT3. **A,** Immunohistochemical staining showed that downregulation of STAT3 (Tyr705) and β-catenin elevated VHL expression in the HJC0152-treated group (scale bar, 100 μm). Hematoxylin and eosin staining was used to examine morphological changes (scale bar, 100 μm). **B,** Immunohistochemical staining showed attenuation of MMP2/9, Ki-67, Cyclin-D1, Bcl-2 in the HJC0152-treated group, accompanied with upregulated cleaved Caspase-3 (scale bar, 100 μm).

expression was also attenuated in HJC0152-treated tumors (Fig. 6C).

Subsequently, IHC staining showed that HJC0152 treatment significantly inhibited total STAT3 or p-STAT3 (Tyr705) expression, elevated VHL expression, and decreased β-catenin expression (Fig. 6A) in SCC25 orthotopic tumors. Collectively, these results suggest that HJC0152 effectively inhibits orthotopic HNSCC tumor growth and invasion *in vivo* through regulating the STAT3/miR-21/β-catenin pathway.

Discussion

The development of effective targeted therapies for the treatment of HNSCC will require in-depth knowledge of the underlying molecular mechanisms of the complex signaling transduction networks involved in cancer development and progression. In the present study, we demonstrated that HJC0152, a novel O-alkylamino-tethered derivative of niclosamide, displayed effective STAT3 inhibitory effects and antitumor effects

against HNSCC. Moreover, we also investigated the mechanism by which HJC0152 suppresses HNSCC proliferation and invasion both *in vitro* and *in vivo*.

Recent research has indicated that abnormal activation of the STAT3 signaling pathway contributes to cancer progression, invasion, chemoresistance, and recurrence (12–14, 40). STAT3 has been shown to be an important transcription factor, and nuclear recruitment of p-STAT3 might trigger transcription of numerous target oncogenes or onco-miRNAs (12–15). Compelling evidence has confirmed that blocking aberrant STAT3 activity is a promising therapeutic strategy for the treatment of solid tumors (41, 42). Meanwhile, preclinical research and clinical trials have revealed that small molecular chemical compound-based therapeutics targeting STAT3 are beneficial in cancer therapy (5–7).

In our *in vitro* experiments with HNSCC cells, HJC0152 inhibited p-STAT3 (Tyr705) to an extent similar to that of STAT3 siRNA. The effects of HJC0152 were dose and time dependent. p-STAT3 (Tyr705) is the most common and important phosphorylated form of STAT3; when it was inhibited, its associated transcriptional activity was also attenuated. First, HJC0152 treatment decreased the invasion and migration ability of SCC25 and CAL27 cells in a dose-dependent manner, which was determined by Transwell and wound-healing assay. Moreover, according to the Transwell assays, we observed that CAL27 cells were more sensitive to HJC0152 than SCC25, in terms of invasion and migration capacity. EMT was widely believed as one of the most important mechanisms in cancer metastasis (33–39), and the EMT process is tightly associated with the loss of membrane localization of E-cadherin and overexpression of N-cadherin (43). Furthermore, Vimentin and Twist-1 also contribute to EMT, and both of them were transcriptionally regulated by STAT3 (28, 44, 45). We therefore measured the expression of E-cadherin, N-cadherin, Vimentin, and Twist-1, and we demonstrated an interrupted EMT process during cancer invasion with HJC0152 treatment. Our results also revealed that both expression and secretion of MMP-2/9, the biomarkers of cell invasion (26, 46–48) and the downstream targets of STAT3 (27–29), were attenuated by HJC0152, suggesting the blockage of extracellular matrix-degrading ability of HNSCC. Finally, we demonstrated that HJC0152 treatment inhibited HNSCC growth through blocking cell cycle at G_1 phase and inducing apoptosis. Cyclin D1 is known as the regulator to switch cell cycle from G_1 to S phase (3) and the downstream target of STAT3 in human cancers (28, 29), and we found decreased Cyclin D1 after HJC0152 treatment in both cell lines, consistent with the cell-cycle analysis. Moreover, decreased Bcl-2 and elevated cleaved Caspase-3 expression suggested that tumor cells' antiapoptosis capacity was inhibited.

MiR-21 has been identified as an onco-miRNA that is overexpressed in many cancers of epithelial origin; therefore, it may be a target with therapeutic potential. Moreover, the upregulated STAT3/miR-21 signaling axis is globally regarded as a negative prognosis predictor in HNSCC, especially in assessing proliferation and metastasis (49). Zhang and colleagues (16) found that the recognition sites for miR-21 are located in the 3′ untranslated region (3′-UTR) of VHL. The authors also demonstrated that VHL is overexpressed after miR-21 abrogation (16). As a downstream target of miR-21, VHL contributes to ubiquitination of β-catenin (16–18), which was involved in the regulation of malignant phenotype in HNSCC (32, 43). Of interest, niclosamide, precursor of HJC0152, was an inhibitory molecule of Wnt/β-catenin signaling (20, 50). In the current study, HJC0152 treatment suppressed miR-21 and β-catenin expression in both cell lines. Moreover, ectogenic miR-21 dramatically inhibited VHL expression and elevated β-catenin expression. In the restoration experiments, we proved that downregulation of VHL partially compensates for the antitumor effect of HJC0152 *in vitro*. These findings suggest that inactivation of STAT3 and the miR-21/β-catenin axis is one of the major underlying mechanisms by which HJC0152 suppresses HNSCC growth and invasion.

The results of our *in vivo* study confirmed our *in vitro* results. HJC0152 treatment inhibited SCC25 cell-derived orthotopic tumor growth and lymph node metastasis. These data suggest that HJC0152 treatment might be a promising approach for the treatment of HNSCC. In the current study, we introduced the HJC0152 into the experimental animals by intraperitoneal injection, which might be the drawback of our *in vivo* test. As shown in our previous report (21), HJC0152 was validated to have better water solubility and oral bioavailability than niclosamide, so more studies with oral administration are warranted for further analysis. Based on these, HJC0152 may have several administration routes in HNSCC clinical therapy.

Taken together, HJC0152 is a small molecular inhibitor that targets STAT3 signaling and miR-21/β-catenin axis. Our results provide a rationale for HJC0152′s clinical applications.

Disclosure of Potential Conflicts of Interest

No potential conflicts of interest were disclosed.

Authors' Contributions

Conception and design: Y. Wang, Y. Wu, L. Zhang, J. Zhou, Q. Shen, X. Zhou
Development of methodology: Y. Wang, Z. Li, X. Yao, C. Zhang, J. Dong, J. Zhou, Q. Shen
Acquisition of data (provided animals, acquired and managed patients, provided facilities, etc.): Y. Wang, S. Wang, Y. Wu, Y. Ren, C. Jing, S. Sun, M. Zhao, W. Guo, X. Qu, Y. Qiao, L. Kong, R. Jin, J. Zhou
Analysis and interpretation of data (e.g., statistical analysis, biostatistics, computational analysis): Y. Wang, Z. Li, X. Yao, J. Dong, S. Sun, M. Zhao, X. Qu, H. Chen, J. Zhou, Q. Shen
Writing, review, and/or revision of the manuscript: Y. Wang, S. Wang, Y. Wu, C. Zhang, N. Ye, K. Zhang, J. Zhou, Q. Shen
Administrative, technical, or material support (i.e., reporting or organizing data, constructing databases): Y. Ren, X. Wang, J. Zhou, Q. Shen
Study supervision: X. Wang, J. Zhou, Q. Shen
Other (synthesized HJC0152): N. Ye

Acknowledgments

The authors thank Jie Zhao at Tianjin Hospital for his kind assistance. We also thank Amy Ninetto, PhD, ELS, Department of Scientific Publications, The University of Texas MD Anderson Cancer Center, for her editing of the manuscript.

Grant Support

This work was supported by the China National Natural Scientific Fund No. 81572492 (X. Zhou), the National Institutes of Health R01 grant DA038446 (J. Zhou), Cancer Prevention Research Institute of Texas award (J. Zhou), the John Sealy Memorial Endowment Fund (J. Zhou), the Institute for Translational Sciences at UTMB (J. Zhou), in part by a Cancer Center Support GrantCA016672 from the NIH/NCI (Q. Shen), Startup fund from MDACC (Q. Shen), Duncan Family Institute Seed Funding Research Program (Q. Shen), and the Holden Family Research Grant in Breast Cancer Prevention, Prevent Cancer Foundation (Q. Shen).

The costs of publication of this article were defrayed in part by the payment of page charges. This article must therefore be hereby marked *advertisement* in accordance with 18 U.S.C. Section 1734 solely to indicate this fact.

Received September 9, 2016; revised December 15, 2016; accepted December 16, 2016; published OnlineFirst January 30, 2017.

References

1. Pulte D, Brenner H. Changes in survival in head and neck cancers in the late 20th and early 21st century: a period analysis. Oncologist 2010;15: 994–1001.
2. Lam L, Logan RM, Luke C. Epidemiological analysis of tongue cancer in South Australia for the 24-year period, 1977–2001. Aust Dent J 2006;51: 16–22.
3. Duan Z, Foster R, Bell DA, Mahoney J, Wolak K, Vaidya A, et al. Signal transducers and activators of transcription 3 pathway activation in drug-resistant ovarian cancer. Clin Cancer Res 2006;12:5055–63.
4. Tong ZT, Cai MY, Wang XG, Kong LL, Mai SJ, Liu YH, et al. EZH2 supports nasopharyngeal carcinoma cell aggressiveness by forming a co-repressor complex with HDAC1/HDAC2 and Snail to inhibit E-cadherin. Oncogene 2012;31:583–94.
5. Cook KM, Figg WD. Angiogenesis inhibitors: current strategies and future prospects. CA Cancer J Clin 2010;60:222–43.
6. Heath VL, Bicknell R. Anticancer strategies involving the vasculature. Nat Rev Clin Oncol 2009;6:395–404.
7. Pan Y, Zhou F, Zhang R, Claret FX. Stat3 inhibitor Stattic exhibits potent antitumor activity and induces chemo- and radio-sensitivity in nasopharyngeal carcinoma. PLoS One 2013;8:e54565.
8. Debnath B, Xu S, Neamati N. Small molecule inhibitors of signal transducer and activator of transcription 3 (Stat3) protein. J Med Chem 2012; 55:6645–68.
9. Gaur AB, Holbeck SL, Colburn NH, Israel MA. Downregulation of Pdcd4 by mir-21 facilitates glioblastoma proliferation in vivo. Neuro Oncol 2011; 13:580–90.
10. Kim N, Kim H, Jung I, Kim Y, Kim D, Han YM. Expression profiles of miRNAs in human embryonic stem cells during hepatocyte differentiation. Hepatol Res 2011;41:170–83.
11. Gabriely G, Wurdinger T, Kesari S, Esau CC, Burchard J, Linsley PS, et al. MicroRNA 21 promotes glioma invasion by targeting matrix metalloproteinase regulators. Mol Cell Biol 2008;28:5369–80.
12. Bourguignon LY, Earle C, Wong G, Spevak CC, Krueger K. Stem cell marker (Nanog) and Stat-3 signaling promote MicroRNA-21 expression and chemoresistance in hyaluronan/CD44-activated head and neck squamous cell carcinoma cells. Oncogene 2012;31:149–60.
13. Wang YY, Sun G, Luo H, Wang XF, Lan FM, Yue X, et al. MiR-21 modulates hTERT through a STAT3-dependent manner on glioblastoma cell growth. CNS Neurosci Ther 2012;18:722–8.
14. Rozovski U, Calin GA, Setoyama T, D'Abundo L, Harris DM, Li P, et al. Signal transducer and activator of transcription (STAT)-3 regulates microRNA gene expression in chronic lymphocytic leukemia cells. Mol Cancer 2013;12:50.
15. Loffler D, Brocke-Heidrich K, Pfeifer G, Stocsits C, Hackermuller J, Kretzschmar AK, et al. Interleukin-6 dependent survival of multiple myeloma cells involves the Stat3-mediated induction of microRNA-21 through a highly conserved enhancer. Blood 2007;110:1330–3.
16. Zhang KL, Han L, Chen LY, Shi ZD, Yang M, Ren Y, et al. Blockage of a miR-21/EGFR regulatory feedback loop augments anti-EGFR therapy in glioblastomas. Cancer Lett 2014;342:139–49.
17. Zhang S, Zhou X, Wang B, Zhang K, Liu S, Yue K, et al. Loss of VHL expression contributes to epithelial-mesenchymal transition in oral squamous cell carcinoma. Oral Oncol 2014;50:809–17.
18. Chen L, Han L, Zhang K, Shi Z, Zhang J, Zhang A, et al. VHL regulates the effects of miR-23b on glioma survival and invasion via suppression of HIF-1alpha/VEGF and beta-catenin/Tcf-4 signaling. Neuro Oncol 2012; 14:1026–36.
19. Dere R, Perkins AL, Bawa-Khalfe T, Jonasch D, Walker CL. beta-catenin links von Hippel-Lindau to aurora kinase A and loss of primary cilia in renal cell carcinoma. J Am Soc Nephrol 2015;26:553–64.
20. Ren X, Duan L, He Q, Zhang Z, Zhou Y, Wu D, et al. Identification of Niclosamide as a New Small-Molecule Inhibitor of the STAT3 Signaling Pathway. ACS Med Chem Lett 2010;1:454–9.
21. Chen H, Yang Z, Ding C, Chu L, Zhang Y, Terry K, et al. Discovery of O-alkylamino tethered niclosamide derivatives as potent and orally bioavailable anticancer agents. ACS Med Chem Lett 2013;4:180–5.
22. Zhou X, Ren Y, Moore L, Mei M, You Y, Xu P, et al. Downregulation of miR-21 inhibits EGFR pathway and suppresses the growth of human glioblastoma cells independent of PTEN status. Lab Invest 2010; 90:144–55.
23. Patel V, Marsh CA, Dorsam RT, Mikelis CM, Masedunskas A, Amornphimoltham P, et al. Decreased lymphangiogenesis and lymph node metastasis by mTOR inhibition in head and neck cancer. Cancer Res 2011; 71:7103–12.
24. Lee TK, Poon RT, Wo JY, Ma S, Guan XY, Myers JN, et al. Lupeol suppresses cisplatin-induced nuclear factor-kappaB activation in head and neck squamous cell carcinoma and inhibits local invasion and nodal metastasis in an orthotopic nude mouse model. Cancer Res 2007;67:8800–9.
25. Chen W, Zheng R, Baade PD, Zhang S, Zeng H, Bray F, et al. Cancer statistics in China, 2015. CA Cancer J Clin 2016;66:115–32.
26. Xie TX, Wei D, Liu M, Gao AC, Ali-Osman F, Sawaya R, et al. Stat3 activation regulates the expression of matrix metalloproteinase-2 and tumor invasion and metastasis. Oncogene 2004;23:3550–60.
27. Dechow TN, Pedranzini L, Leitch A, Leslie K, Gerald WL, Linkov I, et al. Requirement of matrix metalloproteinase-9 for the transformation of human mammary epithelial cells by Stat3-C. Proc Natl Acad Sci U S A 2004;101:10602–7.
28. Basseres DS, Baldwin AS. Nuclear factor-kappaB and inhibitor of kappaB kinase pathways in oncogenic initiation and progression. Oncogene 2006;25:6817–30.
29. Yu H, Kortylewski M, Pardoll D. Crosstalk between cancer and immune cells: role of STAT3 in the tumour microenvironment. Nat Rev Immunol 2007;7:41–51.
30. Yu H, Pardoll D, Jove R. STATs in cancer inflammation and immunity: a leading role for STAT3. Nat Rev Cancer 2009;9:798–809.
31. Kaur J, Sawhney M, DattaGupta S, Shukla NK, Srivastava A, Walfish PG, et al. Clinical significance of altered expression of beta-catenin and E-cadherin in oral dysplasia and cancer: potential link with ALCAM expression. PloS One 2013;8:e67361.
32. Kawakita A, Yanamoto S, Yamada S, Naruse T, Takahashi H, Kawasaki G, et al. MicroRNA-21 promotes oral cancer invasion via the Wnt/beta-catenin pathway by targeting DKK2. Pathol Oncol Res 2014;20:253–61.
33. Brabletz T. EMT and MET in metastasis: where are the cancer stem cells? Cancer Cell 2012;22:699–701.
34. An oncogenic splice variant drives EMT and metastasis in breast cancer. Cancer Discov 2013;3:OF16;DOI: 10.1158/2159-8290.CD-RW2013-027 Published March 2013.
35. Gulhati P, Bowen KA, Liu J, Stevens PD, Rychahou PG, Chen M, et al. mTORC1 and mTORC2 regulate EMT, motility, and metastasis of colorectal cancer via RhoA and Rac1 signaling pathways. Cancer Res 2011; 71:3246–56.
36. Mulholland DJ, Kobayashi N, Ruscetti M, Zhi A, Tran LM, Huang J, et al. Pten loss and RAS/MAPK activation cooperate to promote EMT and metastasis initiated from prostate cancer stem/progenitor cells. Cancer Res 2012;72:1878–89.
37. Parvani JG, Gujrati MD, Mack MA, Schiemann WP, Lu ZR. Silencing beta3 integrin by targeted ECO/siRNA nanoparticles inhibits EMT and metastasis of triple-negative breast cancer. Cancer Res 2015;75:2316–25.
38. Yoo YA, Kang MH, Lee HJ, Kim BH, Park JK, Kim HK, et al. Sonic hedgehog pathway promotes metastasis and lymphangiogenesis via activation of Akt, EMT, and MMP-9 pathway in gastric cancer. Cancer Res 2011;71:7061–70.
39. Byles V, Zhu L, Lovaas JD, Chmilewski LK, Wang J, Faller DV, et al. SIRT1 induces EMT by cooperating with EMT transcription factors and enhances prostate cancer cell migration and metastasis. Oncogene 2012;31:4619–29.
40. Carro MS, Lim WK, Alvarez MJ, Bollo RJ, Zhao X, Snyder EY, et al. The transcriptional network for mesenchymal transformation of brain tumours. Nature 2010;463:318–25.
41. Hedvat M, Huszar D, Herrmann A, Gozgit JM, Schroeder A, Sheehy A, et al. The JAK2 inhibitor AZD1480 potently blocks Stat3 signaling and oncogenesis in solid tumors. Cancer Cell 2009;16:487–97.
42. Liu L, Nam S, Tian Y, Yang F, Wu J, Wang Y, et al. , 6-Bromoindirubin-3′-oxime inhibits JAK/STAT3 signaling and induces apoptosis of human melanoma cells. Cancer Res 2011;71:3972–9.
43. Gonzalez-Moles MA, Ruiz-Avila I, Gil-Montoya JA, Plaza-Campillo J, Scully C. beta-catenin in oral cancer: an update on current knowledge. Oral Oncol 2014;50:818–24.
44. Lo HW, Hsu SC, Xia W, Cao X, Shih JY, Wei Y, et al. Epidermal growth factor receptor cooperates with signal transducer and activator of transcription 3

to induce epithelial–mesenchymal transition in cancer cells via up-regulation of TWIST gene expression. Cancer Res 2007;67:9066–76.
45. Wu Y, Diab I, Zhang X, Izmailova ES, Zehner ZE. Stat3 enhances vimentin gene expression by binding to the antisilencer element and interacting with the repressor protein, ZBP-89. Oncogene 2004;23:168–78.
46. Hastie EL, Sherwood DR. A new front in cell invasion: the invadopodial membrane. Eur J Cell Biol 2016;95:441–8.
47. Shen W, Xi H, Wei B, Chen L. The prognostic role of matrix metalloproteinase 2 in gastric cancer: a systematic review with meta-analysis. J Cancer Res Clin Oncol 2014;140:1003–9.
48. Thakur V, Bedogni B. The membrane tethered matrix metalloproteinase MT1-MMP at the forefront of melanoma cell invasion and metastasis. Pharmacol Res 2016;111:17–22.
49. Zhou X, Ren Y, Liu A, Jin R, Jiang Q, Huang Y, et al. WP1066 sensitizes oral squamous cell carcinoma cells to cisplatin by targeting STAT3/miR-21 axis. Sci Rep 2014;4:7461.
50. Jin Y, Lu Z, Ding K, Li J, Du X, Chen C, et al. Antineoplastic mechanisms of niclosamide in acute myelogenous leukemia stem cells: inactivation of the NF-kappaB pathway and generation of reactive oxygen species. Cancer Res 2010;70:2516–27.